

EXPERIMENTAL INVESTIGATION AND FLOW VISUALIZATION OF STEAM CONDENSATION IN A SCALED IRWST-ADS SIMULATOR

Suleiman Al Issa, and Rafael Macian-Juan

Institute of Nuclear Engineering, Faculty of Mechanical Engineering, Technische Universität München (TUM).

Boltzmann Strasse 15, 85748 Garching b. Muenchen, Germany
salissa.email@gmail.com; rafael.macian@ntech.mw.tum.de

Gonzalo Jimenez, Cesar Queral, and Javier Montero-Mayorga

Universidad Politécnica de Madrid
Avda. Ramiro de Maeztu 7, 28040 Madrid, Spain
gonzalo.jimenez@upm.es; cesar.queral@upm.es; fj.montero@alumnos.upm.es

ABSTRACT

The use of suppression pools to limit the pressure increase in nuclear power plant containments has been a common strategy since the development of the first BWR designs more than 50 years ago. In the new Generation III+ PWR reactors design, suppression pools design has been also incorporated; AP1000 (Westinghouse), EPR (AREVA) and APR1400 (KEPCO). In particular, in an AP1000 design the steam is directly released to the suppression pool from the pressurizer in case of an Automatic Depressurization System (ADS) actuation. . The thermal-hydraulic behavior of the pool is quite complex under accidental conditions: the pool receives steam at high velocity and temperature from the reactor cooling system (RCS), the pool is the heat sink of the Passive Residual Heat Removal (PRHR), and eventually, it is the source for the low pressure safety injection. In order to study the behavior of the AP1000 IRWST during a steam discharge from the ADS at different stages of a SBLOCA, an experimental test rig was constructed in cooperation with the Technical University of Munich (TUM) within the frame of the Spanish Ministry of Economy and Competitiveness research project (Integrated Safety Assessment methodology applied to advanced reactors (ISAMAR)). The experimental test rig consists of a transparent 2.5m vertical channel with a rectangular 15×15 cm cross-section with steam injected vertically from a single injection nozzle near the bottom of the channel. The temperature was monitored at the center of the channel and at different axial locations. Special image-processing programs were implemented to generate 2D time-averaged void fraction distributions at different stages of the experiment. Experiments were performed starting from room temperature until reaching saturation at the top of the channel. The results show that a full condensation occurs as $T < 101.1 \pm 1.9^\circ C$ near the injection. Exceeding this limit, steam bubbles starts to reach the top of the channel, and eventually a local flashing occurred at the last 40 cm of the channel. This implies that a special care should be taken to prevent a large-scale flashing event at the IRWST. The resulting 2D void distributions provide a valuable source for a planned CFD validation.

KEYWORDS

AP1000, IRWST, ADS, SBLOCA, Two-phase flows, flow visualization

1. INTRODUCTION

The use of suppression pools to limit the pressure increase in nuclear power plant containments has been a common strategy since the development of the first BWR designs more than 50 years ago. In the new Generation III+ PWR reactors design, suppression pools design has been also incorporated; AP1000 (Westinghouse), EPR (AREVA) and APR1400 (KEPCO). Within this context of new reactor designs, the Westinghouse AP1000 implements passive safety systems to provide core cooling in case of accidental conditions. Unlike typical safety systems of conventional PWRs, these systems are based on natural forces such as gravity or natural circulation. In order to evaluate their performance and obtain data for computer codes validation, further experimental tests are required. After validation, these codes can be used to reproduce accidental conditions for licensing purposes, and obtain design certification by the U.S. NRC [1-3]. Westinghouse uses NOTRUMP code for AP1000 SBLOCA simulations which was licensed for SBLOCA simulations of standard PWRs in 1985 [4]. NOTRUMP should be further validated against phenomena observed in the AP1000 experiments (Chapter 21, testing and computer code evaluation, final safety evaluation report related to the certification of the AP1000 Standard Design, NUREG-1793, [5]). Within the frame of the Spanish Ministry of Economy and Competitiveness research project (Integrated Safety Assessment methodology applied to advanced reactors: ISAMAR), the nuclear safety group at Universidad Politécnica de Madrid simulated a set of SBLOCA sequences with TRACE code in order to evaluate the performance of passive systems. The results agreed well with the Westinghouse ones calculated using NOTRUMP ([6]). However, the 3D accurate simulation of the thermal-hydraulic behavior of the In-Containment Refueling Water Storage Tank (IRWST) was not possible with TRACE. In case of an Automatic Depressurization System (ADS) actuation in an AP1000, the steam is directly released into the suppression pool from the pressurizer. The thermal-hydraulic behavior of the pool is quite complex under these conditions: the pool receives steam at high velocities and temperatures from the reactor cooling system (RCS). The IRWST serves as the heat sink of the Passive Residual Heat Removal (PRHR) and the water reservoir for the low pressure safety injection system.

The UPM has developed a full containment 3D model with GOTHIC code that has been tested under LBLOCA conditions with adequate results, [7]. But, in a LBLOCA sequence, there is no PRHR and ADS actuation, so the thermal hydraulic behavior of the IRWST is simpler than in a SBLOCA sequence. The right simulation of the IRWST thermal hydraulic behavior is crucial for the correct simulation of the whole AP1000 containment under SBLOCA conditions. Therefore, at this stage of the project it was concluded that more information about the IRWST thermal hydraulic behavior in a SBLOCA was needed in order to set the simulation hypothesis for GOTHIC. For this purpose, an experimental test rig was constructed in cooperation with the two-phase flows laboratory of the institute of nuclear engineering of the Technical University of Munich (TUM).

2. EXPERIMENTS

2.1. Experimental Setup

Figure 1 shows the experimental set-up which consists of the test channel, the steam generator, and an automatic control unit to set the steam mass flow rate at a specific value. The test section consists of a 2.5 [m] long, 0.15×0.15 [m] rectangular channel which has a 0.1 [m] thickness. The volume of the channel was selected for being proportional to each hole in the sparger. The channel is made of a transparent Polycarbonate material which allows optical observation and a continuous operation with temperatures up to 130°C. The top of channel is open and thus excess vapor is vented into the surrounding atmosphere. The steam generator provides a maximum of 10 kW power, which also sets the maximum available steam mass flow rate. The distilled water used to generate the steam is degassed by boiling it for about 30 minutes before the beginning of experiments. The steam leaves the steam generator and passes through a control valve, a cyclone moisture separator, and a vortex flow meter before it enters

the steam injection nozzle. The cyclone separator ensures that only dry steam passes through the flow meter and thus a correct measurement of the mass flow rate can be achieved. A temperature sensor is integrated into the vortex flow meter which allows measuring the temperature of the passing steam and the corresponding steam density (assuming steam in a saturated condition). Consequently, the mass flow rate can be obtained directly from the flow meter. A proportional-integral (PI) feedback control loop receives the measured mass flow rate and change the opening of the control valve to keep the mass flow rate constant at the desired input value. Due to the low mass flow rate, only the average mass flow rate can be kept constant with a small deviation.

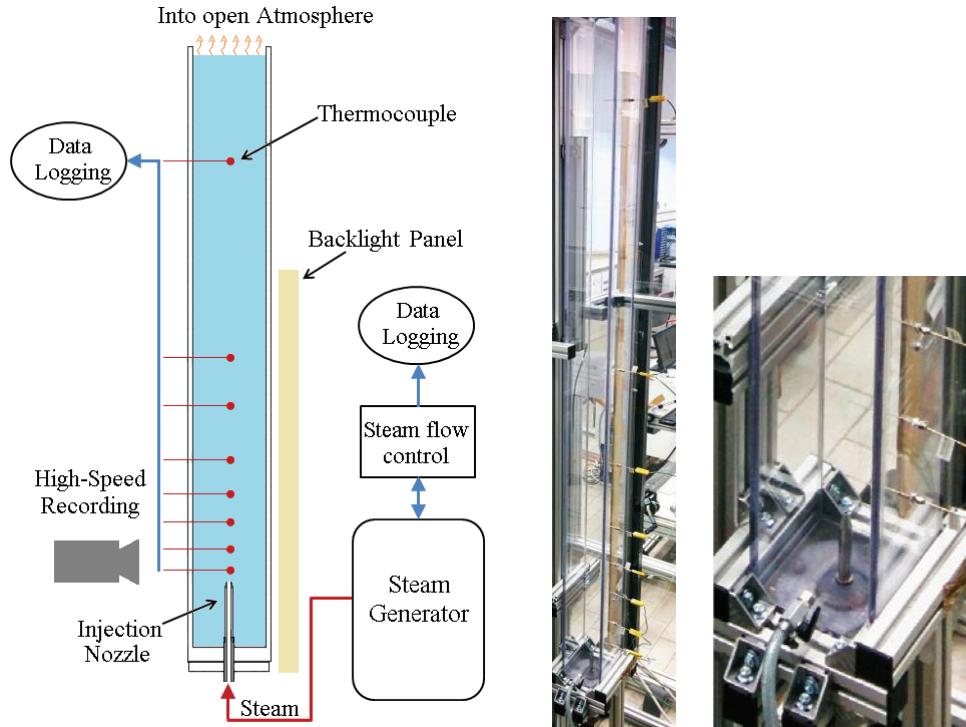


Figure 1. Left: Experimental set-up of the ADS simulator, **Right:** An image that shows the real test section, thermocouples appears to the right side and the steam injection nozzle at the bottom.

The steam was injected via a vertical injection nozzle which has 4 [mm] diameter opening. The nozzle is installed at the center of the channel and the size of the opening was chosen so that it results in a steam output velocity close to the one occurring in realistic ADS sparger's holes. The tip of the nozzle is located about 0.095 m from the bottom of the test section, at a similar distance from the liquid surface to that of the ADS's spargers. A set of eight K-type thermocouples are installed within the test section in order to measure the time development of the axial temperature distribution (figure 1). The thermocouples are built into a 1.5 mm stainless steel envelope, and they are inserted vertically from the side so that the tip of each thermocouple is located at the center of the test channel. The axial distribution of the sensors was chosen so that a finer axial resolution is obtained close to the injection nozzle as shown in figure 1. The distances of the thermocouples from the tip of the injection nozzle were: 0.05, 0.15, 0.275, 0.4, 0.55, 0.8, 1.15, and 2 [m]. The signals from the flowmeter and the thermocouples are recorded via appropriate data acquisition units into the measuring PC, and thus the measured values can be acquired according to a desired sampling rate. Both the steam mass flow rate and temperatures are logged each 1[s] during the experiments. The accuracy of the k-type thermocouples class 1 is ± 1.1 K, however the extension cables from the thermocouples into the data acquisition unit adds an error of ∓ 0.8 K and thus the temperature measurements will have a measuring error of ∓ 1.9 K. The accuracy of

temperature measurement can be improved by calibrating the thermocouples. The steam mass flow rate was measured using a vortex flowmeter with a $\pm 2.55\%$ accuracy.

2.1. High-Speed recording and time-averaged projected void fraction distributions

In order to acquire the steam distribution at different stages, an Imager Pro 4M with max 1279 frame/s @ 2016×2016 pixels high speed camera was implemented. A white backlight 1.16×0.26 m LED panel was used to illuminate the test section. The panel provides a homogenous illumination of 5400 lumen which corresponds to about 10700 lux at a 0.2 m distance from the surface of the panel. The bottom side of the panel was placed at the lower end of the test section which allowed the observation of about 0.9 m of the channel from the bottom of the channel (up to the sixth thermocouple from the bottom). The achieved spatial resolution in current experiments was 1.437 mm/pixel. Own-developed image processing programs [8,9] allow eliminating the background from the raw images, filling white reflections inside bubbles, and removing remaining noise including tiny air bubbles if desired (Figure 2 a,b,c, and d respectively). The result of this procedure is a clean image that includes existing steam or steam bubbles with a white background for water (Figure 2, d). The

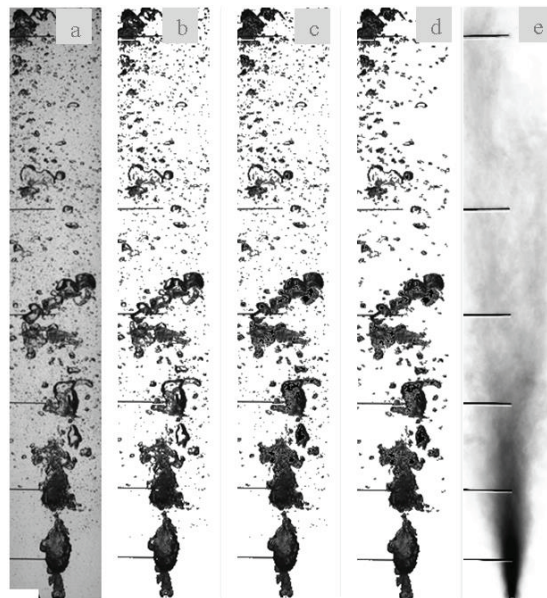


Figure 2. Illustration of the performed image processing: a: Raw image, b: Removing the background, c: Filling of white reflections, d: removing tiny air bubbles, e: time-averaged calculation according to Eq(3).

If the intensity within a processed image at a frame t and a specific location (x, y) was considered as a function:

$$I_t(x, y) \quad (1)$$

The following probability function can be defined:

$$\psi_t(x, y) = \begin{cases} 1 & I_t(x, y) \neq 0 \\ 0 & I_t(x, y) = 0 \end{cases} \quad (2)$$

The time-averaged probability at each pixel will represent the 2D-Projected time-averaged void fraction as follows:

$$\alpha(x, y) = \sum_0^{N_{max}} \frac{\psi_t(x, y)}{N_{max}} \quad (3)$$

Where N_{max} = total number of averaged instances (=3000 in current work). This definition of the void fraction was frequently used to define the local time-averaged void fraction from the data obtained from measuring devices like needle probes. Figure 2(e) shows the result of this calculation. The shadows of existing thermocouples were left to indicate the height and the location of corresponding measured temperatures. The existence of the thermocouples causes a minimal distortion of the main flow due to their small diameter (1.5 mm). If the effect of superposition (existing of bubbles in front each other in the direction of camera) becomes low or negligible, such a distribution can be considered as a good approximation of the time-averaged void fraction within the mid-plane of the channel. This is valid in current experiments when the water temperature is still below the saturation temperature and steam bubbles are detaching one after the other (as a train of bubbles). The over-mentioned-time averaged distribution can still be used as a qualitative evaluation of the time-averaged void fraction distribution when the superposition effect becomes significant.

2.2. Experimental Procedure

As it was mentioned in previous sections, the distilled water used to generate steam is boiled for about 30 minutes. This was done in order to degass the dissolved air. However, dissolved air exists also in the distilled water inside the channel. From preliminary experiments, it was noticed that the dissolved air in the test section water contributes into the amount of tiny air bubbles that appears after the steam condensation. Consequently, the distilled water used for subsequent experiments was also heated up to saturation through continuous injection of steam. The degassed water inside the channel is then left to cool down to room temperature before starting the main experiment. This practice reduced the dissolved air content within the water and provided better conditions for optical observations. For main experiments, the steam mass flow rate was set into the desired value, and the resulting steam is directed initially into a condenser for 30 minutes (degassing). Experiments are then started by directing the steam into the injection nozzle. The time at which the steam starts to appear at the tip of the nozzle is registered as initial time for all measurements. The steam is injected until flashing occurs. During the experiment, several recordings were made using the high speed camera. They were made at different stages of the experiment, and are more frequent as saturation is approached near the highest thermocouple (2 m from the injection nozzle). 14 cases were recorded and these are arranged into 3 stages according to the observed phenomena. Table I shows the temperatures recorded at these 14 cases along with the corresponding saturation temperatures at each elevation (or TC).

Table I. Temperature distribution during HSC-recorded cases

Case #														T_{sat} [°C]
1	2	3	4	5	6	7	8	9	10	11	12	13	14	
t[s]	150	525	1020	1690	2435	3720	4145	4900	5058	5285	5425	5545	5760	5872
TC1	31.0	39.2	47.7	56.8	66.9	83.5	89.1	99.6	101.8	103.1	103.7	103.6	103.8	104.0
TC2	28.7	37.0	45.7	55.0	66.2	82.5	87.6	95.9	97.7	99.7	101.6	101.6	102.6	103.0
TC3	28.0	36.4	44.8	54.2	65.3	82.1	86.9	95.2	97.1	99.3	101.1	101.4	102.1	102.6
TC4	27.3	35.7	43.6	54.0	64.6	81.7	86.4	94.7	95.9	98.2	100.2	101.0	102.0	102.4
TC5	26.4	35.7	42.6	51.9	62.5	78.4	85.0	93.4	95.3	98.2	99.5	99.5	101.6	101.6

TC6	25.9	31.6	42.1	50.3	62.3	78.6	82.8	92.8	94.8	95.1	96.6	98.6	101.3	101.5	102.1
TC7	25.5	29.8	37.4	49.3	58.3	75.5	81.3	90.1	91.7	94.7	96.7	96.6	99.4	100.2	101.3
TC8	25.7	28.1	34.8	45.6	56.2	73.2	78.6	87.2	88.9	90.7	92.5	93.5	96.2	97.8	99.2

2.3. Experimental results

A constant steam mass flow rate of 5.5 kg/h ($\equiv 1.5278 \cdot 10^{-3} \text{ kg/s}$ or $v_{steam,out} = 183.28 \text{ m/s}$) was injected into the channel which was filled with distilled water up to a height of 2.254 m. Figure 3 shows the time development of the injected steam velocity, a nearly constant velocity was provided throughout the experiment.

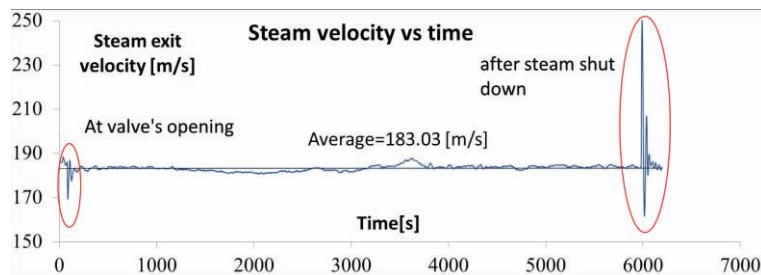


Figure 3. The injected steam velocity during the experiment.

Starting from room temperatures ($\sim 25^\circ\text{C}$), the flow within the test channel goes through different conditions as the water temperature rises. This section will introduce the experimental results categorized according to the range of water temperatures.

2.3.1 Full condensation at the injection nozzle

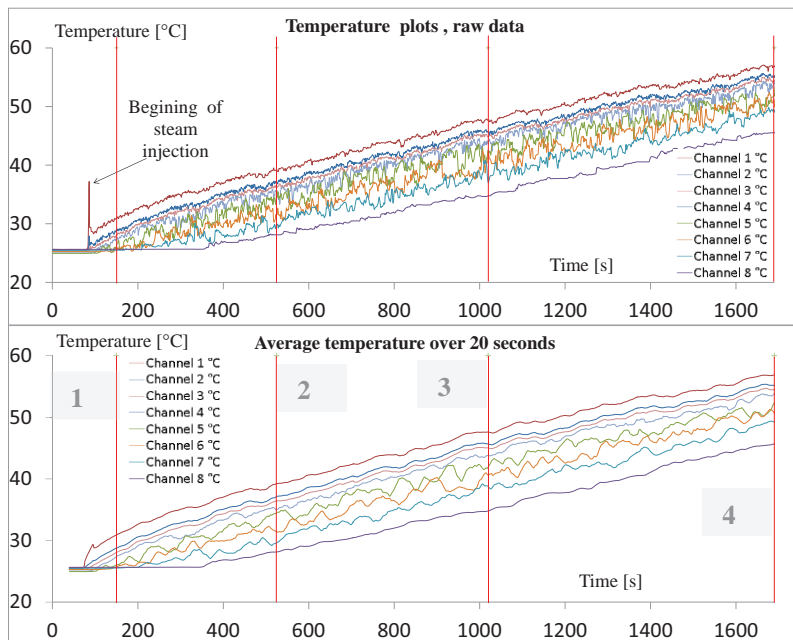


Figure 4. Time development of temperature distribution during the full condensation mode. Upper image: raw temperature measurements, Lower image: averaged temperatures.

Figure 4 shows the time development of water temperature during cases 1-4 of the experiment. During this stage, the water temperature is below 60°C in the test section with a maximum of ~56°C at TC1 and ~45°C at TC8. The steam condenses almost instantly when it comes into contact with water, and a tiny or no steam plume is visible at the injection nozzle (Figure 5). The water heats up due to the development of a natural circulation that is initiated from the start of steam injection. This can be seen from the consecutive initialization of the temperature increase at each of the eight TCs during the first 270 seconds of the experiment (Figure 4). A peak at TC1 can be seen at the beginning of steam injection because of the opening of the steam valve and the sudden injection of a slightly pressurized steam. After this, the steam mass flow rate and pressure stabilize, and the water mixing and recirculation brings the temperature at TC1 into a behavior of a gradual increase. The slightly dark plumes that originate from the injection nozzle in Figure 4, left are due to micro air bubbles resulting from the direct steam condensation at the injection nozzle. The large fluctuations in the temperatures measurement of TC4, TC5, TC6 and TC7 in comparison to TC1, TC2, TC3, and TC8 are thought to come from the moving hot water jet that is rising upwards and fluctuating at medium elevations (TC4-TC7). This oscillating behavior is minimal at lower TCs (TC1-TC3) as the jet velocity is still high. Its effect cannot be seen at TC8 as it widens there to the dimensions of the channels cross section. Figure 5 shows flow conditions during cases 1-4. A tiny steam plume can be noticed in case 4. Direct contact condensation is quite effective in a very short distance from the injection point at high subcooling temperatures and no concerns are present regarding comparable conditions in the IRWST.

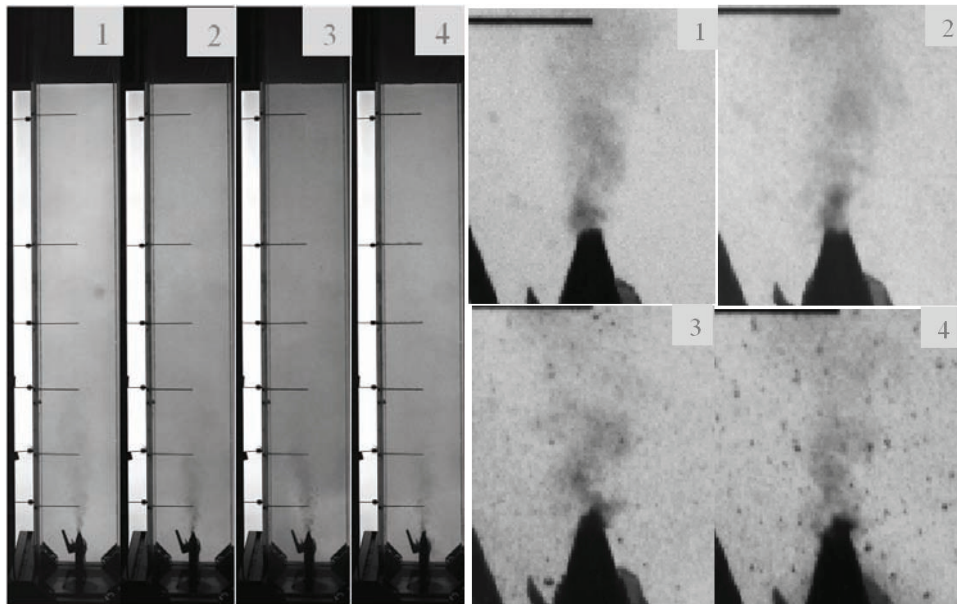


Figure 5. Left: Flow conditions during cases 1-4. **Right:** A closer look of steam direct condensation at the injection nozzle. Steam condenses almost instantly upon contact with highly subcooled water ($T_w < 60^\circ\text{C}$).

2.3.2 Steam flame at the injection nozzle

This stage is characterized by the appearance of a visible steam flame at the nozzle (Figure 6, cases 5-10). A small portion of steam detaches from its top (Figure 6, cases 5 – 10) and the detached single steam bubble condenses fast close to the nozzle as the water temperature around the bubble is still subcooled

(Figure 7, channels 1+2, or see table II cases 5-10). As the steam condenses much slower than in previous stage, this allows the remaining air to form larger bubbles, and these can be clearly seen in figure 7 cases 5-10. Towards the end of this stage, the water temperature starts to approach saturation especially at the lowest thermocouple TC1. This causes slower condensation, and allows the detached steam bubbles to have longer lifetime and travel into higher distances. The steam in this stage condenses completely within the channel and thus no concerns are relevant regarding the performance of the IRWST.

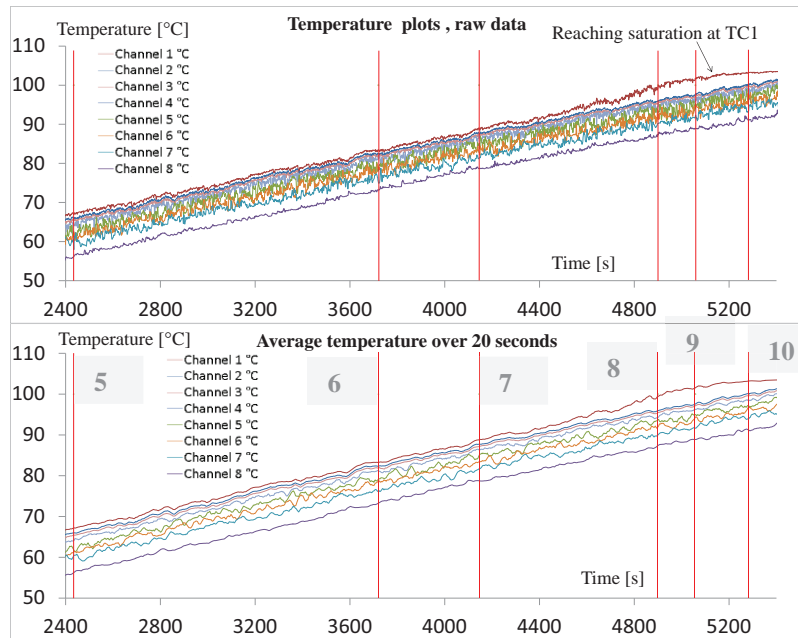


Figure 6. Time development of temperature distribution during second stage

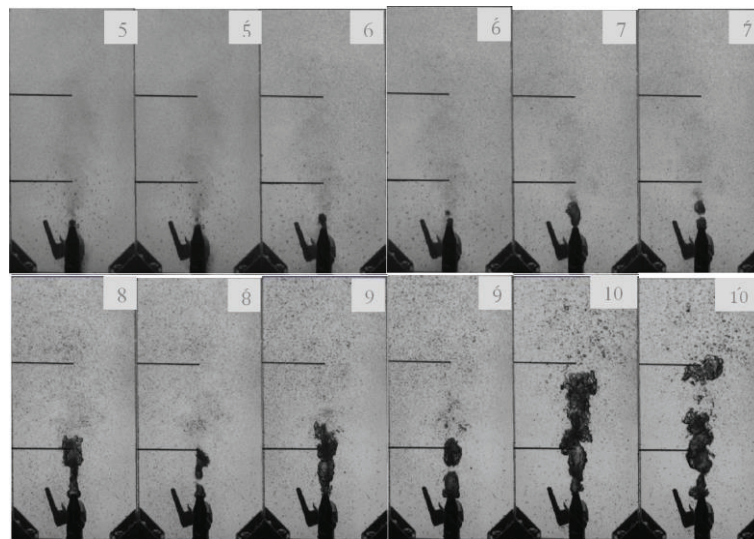


Figure 7. Appearance of a flame at the injection nozzle: cases 5-10. Detachment on a steam bubble from the flame: cases 5 – 10

2.3.3 Steam bubbles rise towards the top of the channel and the occurrence of flashing

This stage of the experiment is the shortest of all observed flow conditions. It lasts for about six minutes during which the water temperature starts to approach the corresponding saturation temperature at each hydrostatic elevation (Figure 8). More steam detaches from the plume, and more than one steam bubble can emerge from detached steam (Figure 9, cases 11-14 and 11 – 14). Steam bubbles condense slowly. They become larger and travel into higher distances transferring the heat upwards and reducing the subcooling temperature along their path. Clusters of mixed bubbles sizes are observed all over the channel (Figure 9, cases 12-14). They move upwards causing more turbulence (bubbles induced turbulence) to be released. Steam bubbles start to reach the top of the channel. These bubbles are small at the beginning, but they become larger as the temperature start to approach saturation near the top of the channel (Figure 8, TC8, and Figure 11). The events accelerate at this point of the experiments, and as the water's temperature below the surface approach saturation, a sudden bulk boiling (flashing) event occurs at the last 30 cm of the test channel. The event is induced by the rising of a swarm of bubbles causing an instant and a local oversaturation in the water close to the surface, where the saturation temperature is at its lowest value. This causes a sudden rise in the void fraction and a large overshoot of water and steam outside the channel (figure 10). In order to prevent further leakage, the steam injection was shut down at this point. Water temperatures decreases instantly after the shutdown of the steam (Figure 8, upper plot, TC1).

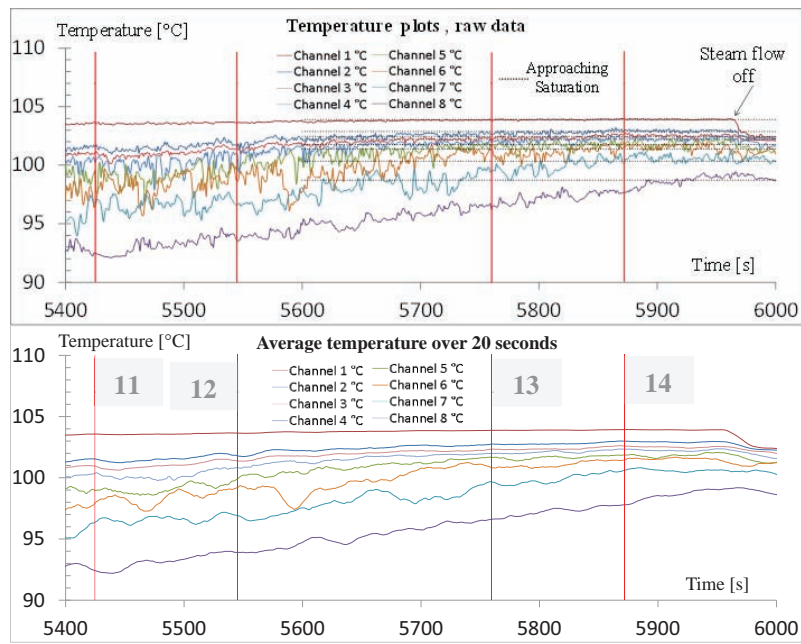


Figure 8. Time development of temperature during cases 11-14.

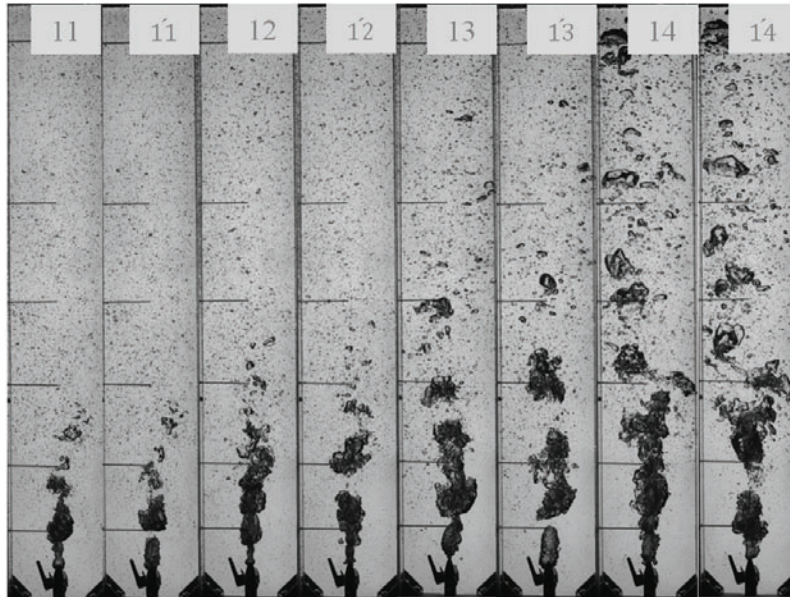


Figure 9. Flow condition during cases 11-14. Steam bubbles condense slowly and rise into higher elevations, the void fraction increases accordingly.

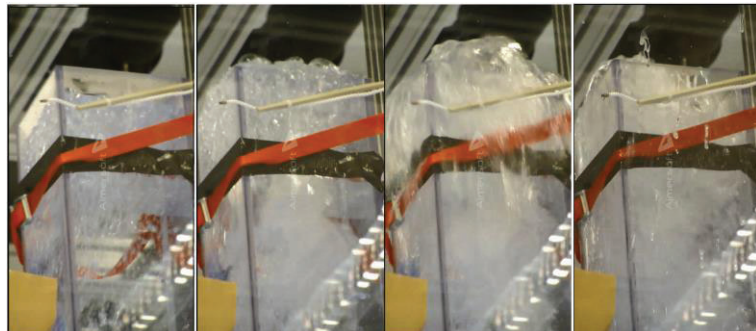


Figure 10. Occurrence of local bulk boiling (flashing) at the last 30 cm of the test section as water temperatures approaches saturation near the top.

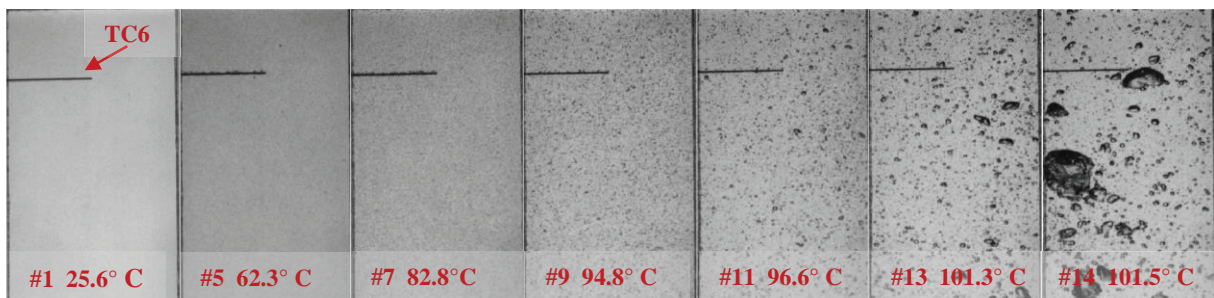


Figure 11 flow condition at the highest recorded TC6 (0.8 m). The saturation temperature at TC6 is $T_{sat} = 102.1^\circ C$.

Figure 11 shows the recorded flow condition at TC6 (0.8 m above the injection nozzle). As it can be seen, some tiny bubbles can be noticed starting from case 7. These are believed to be air bubbles as the steam condense fully at the nozzle. Small steam bubbles can be recognized in case 11. After this point, the size, lifetime, and the elevation at which the steam bubbles arrive start to increase rapidly and clusters of large

and small steam bubbles can be seen in case 14. These swarms of bubbles are responsible for bringing the upper elevations close to saturation at the last stage of the experiment. This stage is the most important one for the IRWST behavior. As saturation temperatures are reached, the direct contact condensation stops to be an effective way of pressure suppression. Steam escapes from the pool without condensing which has a strong implication for the AP1000 IRWST operational limits during a SBLOCA, as the local temperatures must remain below the saturation temperature and the steam need to be condensed in the IRWST to avoid increasing the containment pressure and temperature. This fact can be complicated as the pool is large and the spargers inject steam at two points. Moreover, there is not any forced circulation system and the momentum induced by the steam jets can be insufficient to create a circulation loop in the whole pool geometry. Once saturation conditions are reached near the surface flashing occurs. When the top layer is flashed, the second layer's temperature becomes above saturation point and comes under atmospheric pressure, so it flashes. This effect propagates downwards. As a practical conclusion for the AP1000, once the flashing starts at the upper layers, there is a risk of losing large amounts of the IRWST's inventory in a matter of minutes which could have serious implications from a safety point of view: less inventory available for injection to the vessel in the short term, and pressure and temperature increase in the containment.

2.3.4 Axial temperature and time-averaged projected void fraction distributions

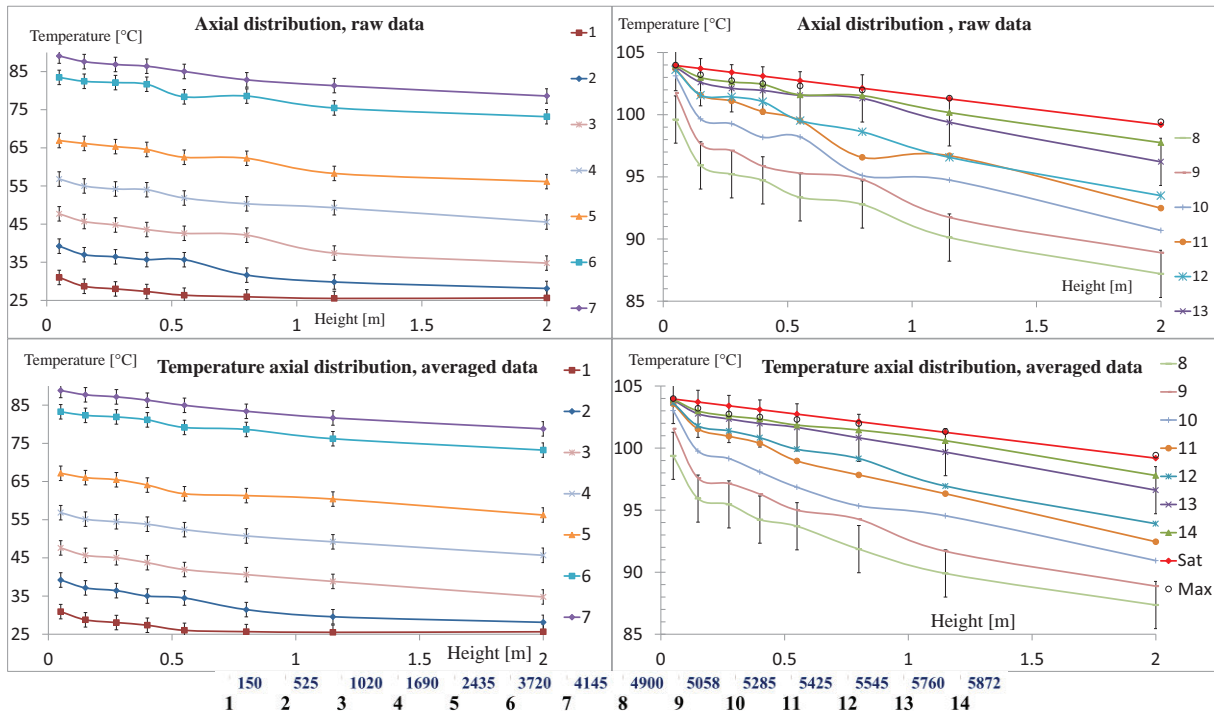


Figure 12 Axial distribution of water temperature. Upper row: Raw data, Lower row: Averaged data over 20 seconds. The lower axis' insert shows the corresponding time (in [s]) for each case. The red line represents the saturation temperature at each elevation. The black circles represent the maximum recorded temperature during the experiment at each measuring TC. In Plots of cases 8-14, errors bars are shown only for cases 8, and 13 in order not to affect plots 'visibility.'

Figure 12, upper row, shows the time development of the axial water temperature distribution for all the eight TCs using raw temperature measurements. Figure 12, lower row, shows the axial distributions using the time-averaged temperature data over 20 seconds. The axial distributions show temperature stratification and a decreasing linear trend, especially when the time-averaged temperature is considered

in cases 1-7. However, some regions with a local temperature maximum appear, and these are more visible within the plots obtained from raw temperature measurements. This phenomenon becomes more pronounced from case 8 onward, and it occurs sometimes at different alternate elevations (cases 9-14). These fluctuations of the axial temperature distributions can be explained by different reasons:

1. Accuracy of the temperature measurements: The amplitude of these fluctuations is of the order of the temperature measuring error (± 1.9 K). This can be seen from the comparison between raw data and averaged data for cases 11+12 in Figure 12. While raw temperature measurements show that case 11 has higher temperatures than case 12 at some elevations (0.55 m and 1.15 m), the average temperature profiles show a more consistent measurements and the entire case 12 profile is higher than the case 11 profile (the same applies for cases 13+14)
2. Flow oscillations of the steam jet caused by steam injection.
3. Sporadic contact of TCs with steam bubbles especially as the bubbles becomes larger and starts to condense slowly.

The oscillating steam jet behavior can be seen from the time-averaged projected void fractions distributions in Figure 14. The jet tends to lean into alternating directions (compare calculated plots cases 11-14, Figure 14). Further PIV measurements should reveal this behavior more accurately. The revelation of the behavior will depends on the used averaging time and the frequency of these oscillations. The water temperature measured at TC1 leaves the general linear trend and shows an accelerated increase after $t=4780$ s (case 8 onward). At this time TC1 comes into a permanent contact with the steam flame and its temperature rises considerably in comparison with other TCs.

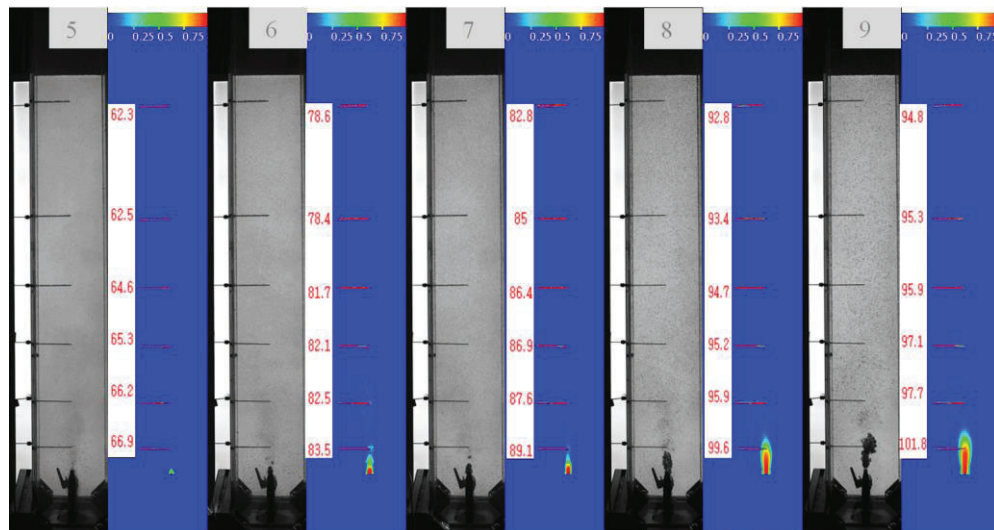


Figure 13 Time-averaged projected void fraction distributions for cases 5-9 along with corresponding temperature measurements in $^{\circ}\text{C}$.

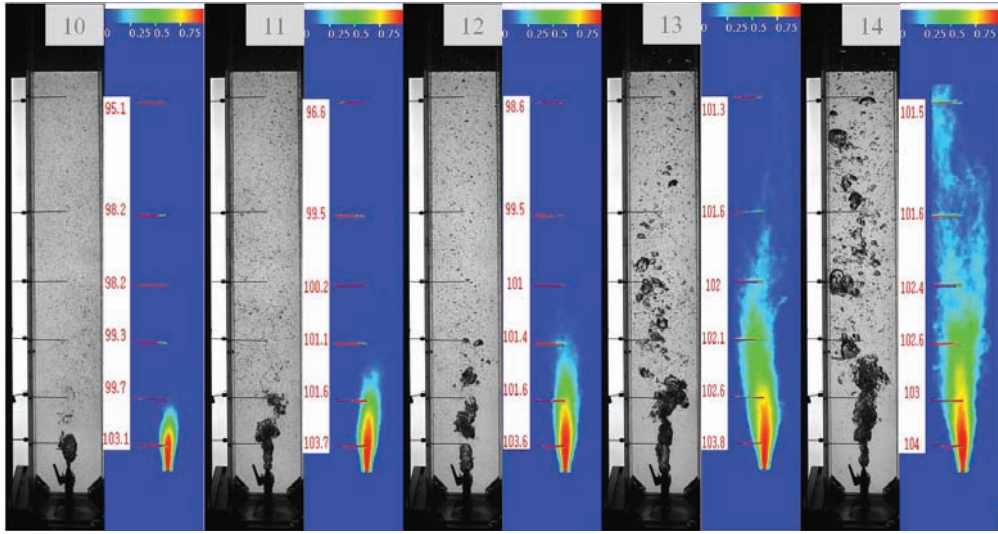


Figure 14 Time-averaged projected void fraction distributions for cases 10-14 along with corresponding temperature measurements in [°C].

Figures 13+14 show the calculated time-averaged projected void fraction distributions according to equation (3) for cases 5-14. Cases 1-4 are not calculated as there is no visible steam flame at the injection nozzle. The flame is tiny for case 5 and grows thereafter. The steam flame takes a regular and a rather a symmetrical shape until case 11. During this time, the temperature at TC1 is still below saturation and relatively small steam bubbles detach from the flame. From case 12 onward, the flame starts to take an irregular shape. This is mainly due to the increased amount of detached bubbles that become larger and travel into higher distances. The amount of increased momentum transfer from the bubbles into the adjacent liquid, (bubble induced turbulence) contributes into the jet's oscillating behavior. The latest flow condition (Figure 14, case 14) is an interesting situation as steam bubbles start to condense very slowly while rising. They create trains of bubbles that transport the heat upwards leading into the flashing event explained in last section. Laurien and Kutnjak [10] noticed that the existence of local temperature maxima (local superheating) can lead into a sporadic occurrence of local bulk boiling. A similar behavior can be noticed in our experiments during case 14 as temperatures approach saturation and it manifests clearly through the flashing event. Figure 12 (Left plots) shows the maximum recorded temperature at each of the eight elevations (black hollow circles). It is clear that saturation temperature is reached at upper TCs (TC6, TC7, and TC8, 0.8, 1.15, and 2 m) as a result of the previously explained phenomena. Although the behavior of the average temperature shows that higher temperatures occurs at lower elevations (due to the proximity to the injection nozzle) and thus the temperatures there are closer to saturation values, this trend is reversed after case 13, and temperatures at higher elevations starts to become closer to the saturation values (case 13+14 Figure 12). The Time-averaged projected void fraction distributions will be needed when comparing to the simulations for choosing the adequate nodalization near the sparger injection in the AP1000 GOTHIC model.

3. CONCLUSIONS

A test rig was constructed in order to investigate the behavior of an AP1000 IRWST during ADS actuators. Steam was injected through a 4 mm opening at the bottom of the test rig producing similar steam exit velocities to those found in a real IRWST. The experimental investigations provided experimental observations, time-averaged 2D distributions of the projected void fraction distributions and temperature axial distributions during different stages of the experiment (different subcooling

temperatures). The results show that the direct contact condensation is not effective as saturation is approached near the steam injection nozzle ($T > 101.1^{\circ}\text{C}$). Steam bubbles of different sizes rise into the top of the rig and the steam is released to the atmosphere. As spargers are not distributed homogeneously in a real IRWST, the local water temperature near the spargers can reach saturation much earlier than the average temperature of the IRWST. In this case, it is possible that the IWRST loses its efficiency in condensing the steam which starts to increase the containment's pressure and temperature during a SBLOCA. When saturation conditions are approached in all the levels above the sparger, flashing occurs near the top and it propagates downwards posing a risk of losing large amounts of the IRWST's inventory in a matter of minutes, lowering the inventory available for core cooling, and rising the containment's pressure and temperature. The data produced by the experiments will be used for the validation of the GOTHIC code and the selection of the adequate simulation hypothesis for the full containment AP1000 model.

ACKNOWLEDGMENTS

This work has been funded by the Spanish Ministry of Competitiveness and Economy within ISAMAR project: ENE2011-28256. Its support is gratefully acknowledged. The authors would also like to thanks to Westinghouse Electric Company and to USNRC for the technical support. The two-phase thermalhydraulic laboratory at the technical university Munich was funded by EON Kraftwerk Germany.

REFERENCES

1. NRC, 1994. SPES-2 RELAP5/MOD3 nodding and 1 Cold Leg break test S00401, Nuclear Regulatory Commission. 22nd Water Reactor Safety information Meeting.
2. Boyack, B., Lime, J., 1995. Analysis of an AP600 Intermediate-size loss-of-coolant accident. In: 7th International Meeting on Nuclear Reactor Thermal-Hydraulics NURETH-7, New York.
3. Corletti, M., 2004. AP1000 Code Applicability Report. Technical Report WCAP15644. Westinghouse Electric Co, LLC. Non-proprietary.
4. Westinghouse, 1985. NOTRUMP Nodal Transient Small Break and General Network Code. Technical Report WCAP-10079-P-A/ WCAP-10080-A. Westinghouse Electric Company. Proprietary/Non-Proprietary versions.
5. NRC, 2004. Final Safety Evaluation Report Related to Certification of the AP1000. Standard Design. NUREG-1793. Nuclear Regulatory Commission.
6. Montero-Mayorga, J., Queral, C., Gonzalez-Cadello, J. AP1000 SBLOCA simulations with TRACE code. Annals of Nuclear Energy 75 (2015) 87–100.
7. Jimenez, G., Bocanegra, R., Fernández, K., Queral, C., Montero, J. Development of a PWR-W and a AP1000 containment building 3D model in a CFD code for Best-Estimate Thermal-Hydraulic Analysis. 22th International Conference on Nuclear Engineering (ICON22), 2014.
8. Al Issa S., Weisensee P., Macián-Juan R. , Experimental investigation of steam bubble condensation in vertical large diameter geometry under atmospheric pressure and different flow conditions, International Journal of Heat and Mass Transfer 70 (2014) 918–929.
9. Al Issa, S., Moreno-Prosper, M., Developing a procedure for calculation of bubble parameters, diameter, velocity, aspect ratio and path depending upon shadowgraph technique and high speed camera recordings for multiple bubbles and diluted bubbly flows. The 15th International Topical Meeting on Nuclear Reactor Thermal - Hydraulics, Pisa, Italy, May 12-17, (2013) .Paper no. NURETH15-045.
10. Eckart Laurien and Josip Kutnjak, Unsteady Bulk Boiling in a Tall and Slender Water Pool, Proceedings of ICAPP 2014, Charlotte, USA, April 6-9, 2014, Paper 14027.